Competitive Adsorption of NO, NO_2, CO_2, and H_2O on BaO(100): A Quantum Chemical Study

Monica Tutuianu,* Oliver R. Inderwildi, Wolfgang G. Bessler, and Jürgen Warnatz

Interdisciplinary Center for Scientific Computing, Heidelberg University, Im Neuenheimer Feld 368, D-69120 Heidelberg, Germany

Received: September 16, 2005; In Final Form: July 13, 2006

Density functional theory (DFT) quantum chemical calculations are used to determine adsorption energies and geometries of NO, NO_2, CO_2, and H_2O on a barium oxide (100) surface. The study includes two adsorption geometries for NO_2. All species form thermodynamically stable adsorbates, and adsorption strength increases in the order $NO_2 < H_2O < NO \leq CO_2$. The influence of surface coverage on adsorption energy is investigated for all species, and a strong coverage dependence is observed. For CO_2, a chemisorbed, carbonate-type structure is identified; the adsorption from the gas phase is nonactivated. Numerical calculations of the competitive adsorption/desorption equilibria of the four species show that, under typical engine exhaust gas composition, the BaO surface is carbonated to a large extent. The results indicate that carbon dioxide plays an essential role in the surface processes during NO_x storage on BaO, where it can block a large part of available surface sites.

1. Introduction

Storage catalytic converters based on barium compounds are a technology with promising potential for the abatement of nitric oxides (NO_x) from lean-burning engine exhaust.[1,2] The operation is based on periodic long lean (storage of NO_x into the catalyst) and short rich (release of NO_x from the catalyst and reduction) engine combustion phases. However, despite considerable research effort, the chemical-mechanistic details of these storage and release processes are not very well understood.[3−7] The nature of the active storage sites (barium oxide, barium hydroxide, barium carbonate, or other compounds) remains an open question.[8] Gas-phase species present under real operating conditions such as carbon dioxide (CO_2) and water (H_2O) may influence the nature of the storage site, even if they are not directly involved in the storage process. While many laboratory studies were performed using model exhaust gases ($NO_x/N_2/O_2$),[9−12] others include CO, CO_2, and/or H_2O[13,14] or use real engine exhaust gas.[15]

Thermodynamic bulk properties have been used to assess the stability of the various barium phases,[8,15,16] but the results are not conclusive for several reasons: (1) The free-enthalpy difference between several bulk phases (nitrate/carbonate) is close to zero at realistic operation conditions, (2) NO_x storage is primarily a surface and subsurface effect, so that the relevance of bulk-phase calculations is unclear, and (3) under typical transient operation conditions, bulk-phase transitions are kinetically controlled, so that the use of thermodynamical data may not be valid. Therefore, understanding the surface rather than the bulk-phase kinetics and thermodynamics is of high importance for understanding NO_x storage.

Quantum chemical calculations by means of density functional theory (DFT) have proven a valuable tool for investigating surface processes.[17,18] They have been used previously to study NO_x interaction with BaO surfaces using either periodic-slab calculations[16,19−21] or cluster calculations.[22−24] While these studies have already allowed a detailed insight into surface processes involved in NO_x storage, they leave open a number of important issues: (1) the dependence of the adsorbate−surface interaction on surface coverage is not considered, and this may partly explain the discrepancies in the results presented so far; (2) the studies do not include water as adsorbate, which is, however, present in major quantities in engine exhaust gas; (3) the consequences of the obtained results for surface reactivity are not discussed quantitatively.

To bring more light into these questions, we performed quantum chemical studies of adsorption of the relevant gas-phase species NO, NO_2, CO_2, and H_2O on BaO(100) surfaces using periodic-slab DFT calculations. BaO(100) is chosen as a model surface for NO_x storage for several reasons: (1) laboratory studies have shown that BaO is indeed a material with storage capacity,[4] (2) the previous DFT studies can serve as reference work, and (3) it has a lower structural complexity of BaO compared to other compounds (e.g., $BaCO_3$[16]). This paper presents DFT calculations of adsorption geometry and adsorption energy of NO, NO_2, CO_2, and H_2O in dependence on adsorption site and surface coverage. Activation energies are determined for transitions between gas-phase and chemisorbed species. Numerical calculations of the competitive adsorption/desorption equilibria of the four species are carried out in order to quantify the surface coverages under realistic exhaust gas conditions.

2. Method

Density functional theory (DFT) ab initio calculations are becoming a useful tool for estimating thermodynamic and kinetic parameters for detailed surface reaction mechanisms. Its absolute accuracy for adsorption and activation energies, based on state-of-the-art functionals, is estimated to be on the order of tenths of an electronvolt.[17,18,25] It can successfully predict trends and relative stabilities. Its versatility in the choice of substrate (oxidic, metallic) and adsorbate (atomic, molecular) makes it particularly valuable when information is not easily accessible

* Corresponding author. E-mail: monica.tutuianu@iwr.uni-heidelberg.de. Telephone: +49 6221 548892. Fax: +49 6221 548884.

10.1021/jp055268x CCC: $33.50
Published on Web 08/15/2006

TABLE 1: Surface Relaxation after Geometry-Optimizing the First Two Atomic Layers of a Five-Layer BaO Slab in a (1 × 1) Supercell

	O_{surf} site in top layer (pm)	Ba_{surf} site in top layer (pm)
top layer−2nd layer	262.7	268.2
2nd layer−3rd layer	285.9	282.0
3rd layer−4th layer	278.1[a]	278.1[a]
4th layer−5th layer		

[a] (= bulk distance).

with conventional experimental techniques (e.g., surface diffusion coefficients, coverage dependence of thermodynamic parameters[26]). In the present work, DFT calculations were performed using the Cambridge Sequential Total Energy Package (CASTEP).[27] The general gradient approximation (GGA), as proposed by Perdew and Wang,[28] was applied, combined with Vanderbilt ultrasoft pseudopotentials.[29] The plane wave basis set was truncated at a kinetic energy of 300 eV, and the *k*-points spacing was set to 5 pm^{-1} within the Brillouin zone as generated by the Monkhorst−Pack scheme.[30] Because of its minor influence on calculated adsorption energies, spin effects were neglected (see below). To understand electronic effects between the surface and the adsorbed molecules, Mulliken charge transfer was calculated according to a formalism described by Segall et al.[31]

CASTEP applies three-dimensional periodic boundary conditions around one unit cell (supercell). In this unit cell, we represent the BaO surface as a slab consisting of 4 atomic layers, extending by symmetry to an infinite surface. The slab structure was obtained by the following procedure: Bulk BaO was geometry-optimized, and a five-layer slab was cleaved. The positions of the upper two atomic layers of this slab were geometry-optimized, leading to considerable surface relaxation (Table 1). The upper four atomic layers of the optimized slab were used for all subsequent calculations with fixed atomic coordinates. The distance between the slabs (vacuum thickness = size of unit cell perpendicular to slab−slab thickness) was set to 1000 pm. Calculated NO_2 adsorption energies showed variations ≤0.1 eV for vacuum thicknesses between 800 and 1500 pm. Adsorbate coverages were varied by choosing various lateral sizes of the supercell. In particular, coverages θ of 0.5, 0.25, and 0.125 were obtained by studying single molecules adsorbed on the center atom of a (1 × 1), ($\sqrt{2} \times \sqrt{2}$), and (2 × 2) unit cell, respectively.

To determine adsorption energies E_{ads}, three single-point (total) energy calculations are needed: (1) surface slab without adsorbate, (2) surface slab with adsorbate after geometry optimization of the adsorbate, and (3) gas-phase adsorbent molecule after geometry optimization. The adsorption energies were calculated according to

$$E_{ads} = E_{(slab+adsorbate)} - (E_{slab} + E_{adsorbent}) \quad (1)$$

To determine activation energies, the transition state of the reaction was located on the potential energy hypersurface (PES) by performing a linear synchronous combined with a quadratic synchronous transit calculation and conjugate gradient refinements[32] as implemented in CASTEP. The activation energy E_{act} is obtained as the difference between calculated reactant and transition state energies.

The calculation methodology outlined above relies on two simplifying assumptions, that is, (1) the disregard of spin effects and (2) the use of a frozen slab for calculations with adsorbates. These assumptions are necessary in order to keep computation times to a reasonable limit, given the large number of different adsorbates and surface coverages investigated here. This is true in particular for PES calculations. To justify these assumptions, we performed a set of calculations for an NO_2 molecule on a BaO surface using a (1 × 1) supercell where the assumptions were consecutively relaxed. The results are given in Table 2. In all cases, the adsorbed molecule was geometry-optimized, using either (a) a frozen slab cleaved from the bulk geometry without further optimization, (b) the frozen slab used throughout the present paper (cf. above), (c) additional relaxation of the surface adsorption site atom, or (d) additional relaxation of the complete first slab layer. The adsorption energy gained by full relaxation in comparison to the fully nonrelaxed surface is ∼0.25 eV. In all cases, spin-polarized (DFT-GGSA) and unpolarized (DFT-GGA) calculations resulted in a difference in adsorption energies of only 0.1 eV and almost insignificant difference in the geometry of adsorbed molecule. The same influence of spin effects was obtained for NO_2 adsorption on larger supercells and also for NO. It is also in agreement with earlier studies of NO on Rh(111).[33] It is interesting to note that the energy gain from additional surface relaxation is to a large extent canceled by the energy loss due to inclusion of spin effects.

Given these results, we believe that the uncertainty induced from the assumptions is only minor and does not affect the conclusion drawn within the present paper. Not only is it within the absolute accuracy of DFT, it is also considerably less than the variation of adsorption energies for different adsorbates or for one adsorbate at different coverages, as will be shown in the following sections.

3. Results

3.1. Bulk and Gas-Phase Species. The bulk geometry of cubic barium oxide, as well as the geometries of the various

TABLE 2: Influence of Surface Relaxation and Spin Polarization on the DFT Results of a Geometry-Optimized NO_2 Molecule Adsorbed on a BaO(100) Surface in a (1 × 1) Supercell

investigated cases of surface relaxation	*a*		*b*		*c*		*d*	
functional	GGA	GGSA	GGA	GGSA	GGA	GGSA	GGA	GGSA
adsorption energy (eV)	−0.6	−0.5	−0.7	−0.6	−0.8	−0.7	−0.8	−0.7
distance O_{surf}−NO_2 (pm)	229.3	229.3	236.7	234.5	253.1	250	246.5	245.2
distance O−NO (pm)	123.7	123.6	123.8	123.8	124.1	124.2	124.6	124.5
angle ONO (deg)	128.6	128.8	127.9	127.6	126.6	126.6	125.7	125.6
Mulliken charge analysis. Net electron transfer to adsorbate (e)	−0.3	−0.3	−0.4	−0.4	−0.4	−0.4	−0.5	−0.5
interlayer distance Ba_{surf} (top layer)−O (2nd layer) (pm)	276.1	276.1	268.2	268.2	268.2	268.2	288.1	285.7
interlayer distance O_{surf} (top layer)−Ba (2nd layer) (pm)	276.1	276.1	262.7	262.7	243.5	245.8	249.5	250.5

[a] Frozen slab cleaved from the bulk geometry without further optimization. [b] Geometry-optimized (cf. Table 1) and subsequently frozen slab. [c] Additional relaxation of the surface adsorption site atom. [d] Additional relaxation of the complete first slab layer. GGA = general gradient approximation, GGSA = general gradient spin approximation. Case (b)/GGA corresponds to the calculations performed throughout the remainder of this paper.

TABLE 3: Comparison of DFT-Calculated Bulk and Molecular Geometries with Reported Experimental Values

	this work		experiment[35,48]	
	bond distance (pm)	bond angle (deg)	bond distance (pm)	bond angle (deg)
BaO (bulk, cubic)	278		276	
NO (gas)	118.6		114	
NO_2 (gas)	122	133.7	120	134
CO_2 (gas)	117	179.9	116	180
H_2O (gas)	97	105.1	96	104.5

adsorbents investigated, were optimized using the DFT method described above. The results are given in Table 3. The calculated bond distances and angles agree within 2% with reported experimental values.

3.2. Nitrogen Monoxide (NO) Adsorption. Experiments[4,34] and DFT studies[20,24] have shown that nitric oxide adsorbs on barium oxide as nitrite-like species over an O_{surf} site. We use DFT to investigate the coverage-dependence of NO molecular adsorption on the BaO(100) surface.

Figure 1 shows the optimized geometry of an adsorbed NO molecule in a (1×1) supercell (coverage $\theta = 0.5$). The adsorption energy is plotted versus coverage for coverages θ of 0.5, 0.25, and 0.125 in Figure 2, and geometric, energetic, and charge-transfer values are given in Table 4. The results show a strong interaction of the molecule with the basic surface anion even at high coverage ($E_{ads} = -1.0$ eV at $\theta = 0.5$), with almost linearly decreasing adsorption energy for decreasing coverage ($E_{ads} = -1.5$ eV at $\theta = 0.125$). The high adsorption energies, relatively short distance from the surface ($d(N-O_{surf}) = 147.8$ pm at $\theta = 0.125$), and an $O_{surf}-N-O$ angle of 110° support the nitrite-like nature of this species (cf. free nitrite anion:[35] $d(N-O) = 123.6$ pm, ONO = 115°).

The strong NO interaction with the surface is further supported by the Mulliken charge analysis performed, which shows a high net electron transferred from the surface to the molecule. The NO adsorption energy versus net electron transferred from the surface to the adsorbate is shown in Figure 3.

3.3. Nitrogen Dioxide (NO_2) Adsorption. Molecular adsorption of NO_2 on BaO is believed to be the first step involved in the overall NO_x storage mechanism.[6,15] Various adsorbate geometries have been identified both experimentally[3,34] and via quantum chemical calculations[20,21] (see Section 4.1 for a more detailed discussion), including N- or O-bonded adsorbates,

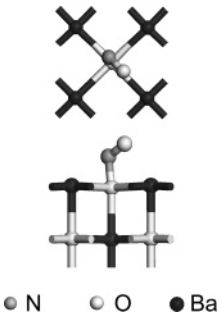

Figure 1. Optimized structure of NO adsorption on BaO(100) surface.

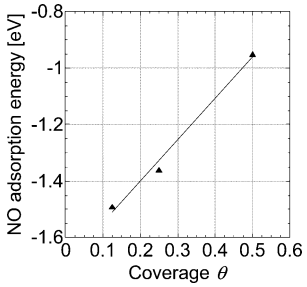

Figure 2. Coverage dependence of NO adsorption energy. The line represents a linear fit (cf. Table 5).

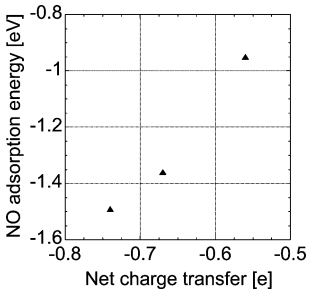

Figure 3. NO adsorption energy dependence on the net electron transfer.

TABLE 4: DFT Calculation Results for the Various Species and Geometries Investigated in This Work

adsorbate structure	distance surface atom−adsorbate atom (pm)	bond distance within adsorbate (pm)	bond angle of adsorbate (deg)	adsorption energy (eV)	Mulliken charge analysis. Net electron transfer to adsorbate (e)
NO, $\theta = 0.125$ (Figure 2)	147.8	129.7	109.7	−1.5	−0.8
NO, $\theta = 0.25$ (Figure 2)	147.8	128.9	109.8	−1.4	−0.7
NO, $\theta = 0.5$ (Figures 1, 2)	154.3	126.5	108.1	−1.0	−0.6
NO_2-Ba_{surf}, $\theta = 0.125$ (Figure 5)	361.3	126.3	120.0	−1.3	−0.6
NO_2-Ba_{surf}, $\theta = 0.25$ (Figure 5)	358.5	125.1	122.9	−0.9	−0.5
NO_2-Ba_{surf}, $\theta = 0.5$ (Figures 4, 5)	355.4	124.0	125.8	−0.6	−0.3
NO_2-O_{surf}, $\theta = 0.125$ (Figure 5)	233.2	125.2	124.4	−1.1	−0.6
NO_2-O_{surf}, $\theta = 0.25$ (Figure 5)	234.9	124.6	126.1	−0.9	−0.5
NO_2-O_{surf}, $\theta = 0.5$ (Figures 4, 5)	236.7	123.8	127.9	−0.7	−0.4
CO_2, $\theta = 0.5$ (Figure 7(1))	404.5	116.9	179.5	−0.1	0
CO_2, $\theta = 0.5$ (Figure 7(2))	278.0	117.5	168.8	−0.2	−0.2
CO_2, $\theta = 0.125$ (Figure 8)	140.6	125.5	125.8	−1.7	−0.8
CO_2, $\theta = 0.25$ (Figure 8)	142.3	124.9	127.5	−1.4	−0.8
CO_2, $\theta = 0.5$ (Figures 7(3), 8)	147.1	123.6	131.6	−0.8	−0.6
H_2O, $\theta = 0.125$ (Figure 11)	104.8	97.0 (O−H[a]) 145.9 (O−H[b])	126.2	−1.5	−0.4
H_2O, $\theta = 0.25$ (Figure 11)	106.5	97.0 (O−H[a]) 141.1 (O−H[b])	124.0	−1.1	−0.3
H_2O, $\theta = 0.5$ (Figures 10, 11)	108.7	96.7 (O−H[a]) 137.8 (O−H[b])	117.2	−0.9	−0.3

[a] Upper H atom. [b] Lower H atom.

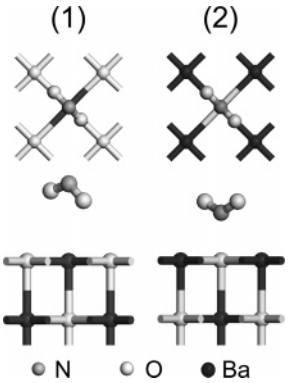

Figure 4. Optimized structures of NO_2 adsorbed on BaO(100) surface. Geometries for a surface coverage of $\theta = 0.5$. Structure (1) represents adsorption over a Ba_{surf} site and structure (2) represents adsorption over an O_{surf} site.

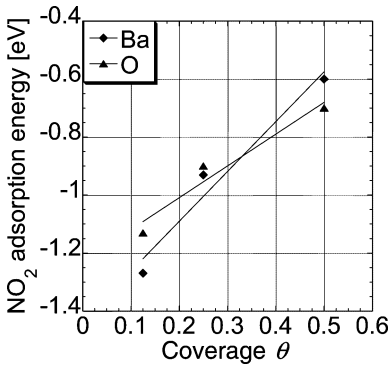

Figure 5. Coverage dependence of NO_2 adsorption energy over a Ba_{surf} site and an O_{surf} site. The lines represent linear fits (cf. Table 5).

bridged chelate-type structures, and adsorption over either barium or oxygen surface sites (Ba_{surf} or O_{surf}, respectively). We have investigated the stability of two representative adsorption geometries, an $O_{surf}-NO_2$ species and a $Ba_{surf}-O_2N$ chelate-type species. The optimized geometries are shown Figure 4 for a (1 × 1) supercell ($\theta = 0.5$). In both cases, the NO_2 molecule interacts strongly with the BaO(100) surface, forming stable adsorbates ($E_{ads} = -0.6$ eV for adsorption over a Ba_{surf} atom and $E_{ads} = -0.7$ eV adsorption over an O_{surf} atom) with relatively long distances above the surface ($d(Ba_{surf}-N) = 355.4$ pm; $d(O_{surf}-N) = 236.7$ pm). Geometrical values of the optimized structures are given in Table 4.

The influence of surface coverage on adsorption energy was studied for coverages θ of 0.5, 0.25, and 0.125. The results are shown in Figure 5, and geometric, energetic, and charge-transfer values are given in Table 4. The calculations show a strong dependence of adsorption energy on coverage, with the energy generally decreasing (i.e., the adsorbed molecule becoming more stable) with decreasing coverage. Calculated adsorption energies reach values down to −1.3 eV for the lowest investigated coverage ($\theta = 0.125$). Results of a Mulliken charge analysis are shown in Figure 6. The adsorption energy increases linearly with increasing net charge transferred from the BaO surface to the adsorbed NO_2 molecule.

3.4. Carbon Dioxide (CO_2) Adsorption. Molecular adsorption of CO_2 on BaO represents a first step in the formation of carbonates. Using cluster DFT calculations, Karlsen et al.[23] observed two different adsorbate configurations for CO_2 on metal oxides: a strongly adsorbed (chemisorbed) species with nonlinear geometry on BaO, and a weakly adsorbed (physisorbed), almost linear species on MgO. In initial calculations for BaO on a (1 × 1) supercell ($\theta = 0.5$), we were able to

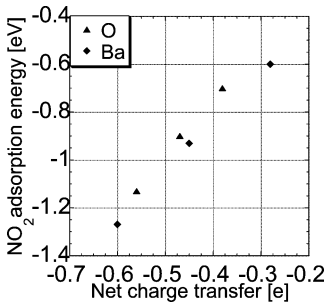

Figure 6. Dependence of NO_2 adsorption energy over Ba_{surf} and O_{surf} sites on the net electron transfer.

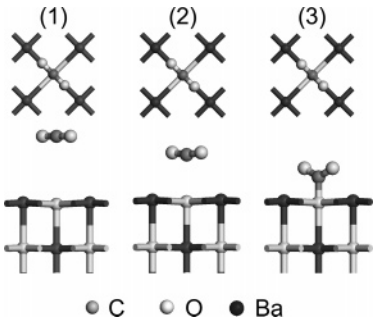

Figure 7. Geometry of the three investigated adsorbate states of molecular CO_2: (1) gas-phase, (2) physisorbed, (3) chemisorbed, carbonate-type species.

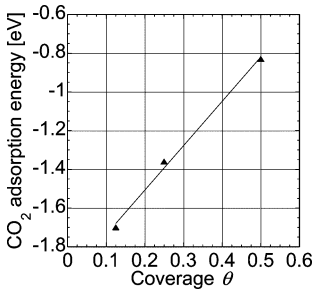

Figure 8. Coverage dependence of CO_2 adsorption energy. The line represents a linear fit (cf. Table 5).

reproduce both geometries. The structures are shown in Figure 7, together with a gas-phase type species. Geometric, energetic, and charge-transfer values of these structures are given in Table 4. The chemisorbed species is very stable ($E_{ads} = -0.8$ eV). It has a carbonate-type structure involving one surface O atom ($d(O_{surf}-C) = 147$ pm, $d(O-C) = 123$ pm, OCO = 131.6°; cf. carbonate:[35] $d(O-C) = 130$ pm, OCO = 120°). The calculations thus indicate the formation of a surface carbonate.

To get more information on the CO_2 adsorption kinetics, the energy of the transition states for transitions between structures 1−2 and 2−3 shown in Figure 7 was calculated. The analysis yielded nonactivated adsorption ($E_{act} < 0.01$ eV for both transitions, which is smaller than the accuracy that can be expected for DFT calculations). The fact that the physisorbed structure is observed as a stable structure at all in the calculations is probably connected to the fact that the DFT calculations represent $T = 0$ K conditions. Thus, the physisorbed-type species is metastable at 0 K and unstable at high temperatures. Exposure of the surface to CO_2 will lead directly to surface carbonate-type species formation.

The coverage dependence of the CO_2 adsorption energy (carbonate-type structure) is shown in Figure 8, and additional data is given in Table 4. The adsorption energy decreases strongly (i.e., the adsorbed molecule becomes more stable) with

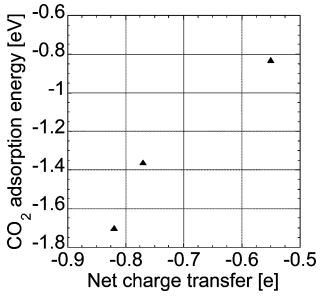

Figure 9. CO_2 adsorption energy dependence on the net electron transfer.

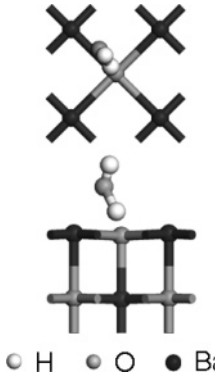

Figure 10. Optimized geometry of adsorbed water.

decreasing coverage, as in the case for NO_2 adsorption, reaching adsorption energies of -1.7 eV for the lowest investigated coverage ($\theta = 0.125$). The CO_2 adsorption energy versus net charge transferred from the surface to the adsorbate, according to a Mulliken population analysis, is shown in Figure 9. Similar to NO_2 adsorption, the net electron transfer decreases with increasing coverage, but the effect is stronger for the CO_2 molecule. This confirms the strong electronic interaction of this molecule with the surface.

3.5. Water (H_2O) Adsorption. In humid atmospheres, the surface of oxidic substrates is usually considered to be completely saturated with H and OH molecules.[36] This is due to the highly Lewis-basic and -acidic character of the free surface oxygen and metal ions, respectively. There are, to the best of our knowledge, no DFT studies of water adsorption on BaO surfaces. However, H_2O on magnesium oxide (MgO) has been intensively investigated both experimentally[37] and theoretically,[38−41] and it was observed that water can adsorb both molecularly and dissociatively.

We have calculated adsorption geometry and energy of adsorbed H_2O in dependence on surface coverage. Various different adsorption configurations (molecular and dissociative adsorption over different sites) were investigated. The optimized geometry of the most stable structure on a (1×1) supercell is shown in Figure 10, and geometrical parameters are given in Table 4. We observe a strong adsorption energy ($E_{ads} = -0.9$ eV) in the same range as for NO and CO_2. The optimized geometry has a short distance above the surface ($d(HOH-O_{surf}) = 108$ pm, $d(H_2O-Ba_{surf}) = 259$ pm), one short OH bond typical for an H_2O molecule ($d(H-OHO_{surf}) = 97$ pm), and a second, elongated OH bond ($d(HO-HO_{surf} = 137$ pm). The structure thus represents a partially dissociated water molecule forming a stable complex with O_{surf} and Ba_{surf} sites. We have also calculated the adsorption energy of a fully dissociated structure ($HO-Ba_{surf}$ and $H-O_{surf}$). It varies between 0.1 and 0.5 eV for $\theta = 0.5-0.125$ and is therefore considerable less stable. Hydrogen bonding between coadsorbed water molecules[42] could not be identified in the present study. Note, however, that adsorption behavior can be different at stepped surfaces.[24,43] The adsorption/dissociation behavior of water on oxidic surfaces is complex, and a full understanding of these effects would require further investigations, which are beyond the scope of the present study.

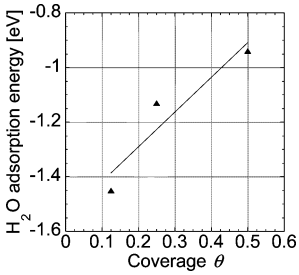

Figure 11. Coverage dependence of H_2O adsorption energy. The line represents linear fit (cf. Table 5).

The influence of surface coverage on adsorption energy of the stable structure is shown in Figure 11. As in the case for NO, NO_2, and CO_2, a strong dependence is observed, with adsorption energies becoming more stable with decreasing coverage. At high surface coverage $\theta = 0.5$, the adsorption energy is -0.9 eV, while for the lowest investigated coverage $\theta = 0.125$, an adsorption energy of -1.5 eV is obtained. The strong H_2O interaction with the BaO surface is further supported by a Mulliken charge analysis. The values for the electron transfer from the surface to the adsorbate are given in Table 4. A higher net electron donation is observed with decreasing surface coverage. The electron donation is lower than the one observed for NO, NO_2, and CO_2.

Various geometries of the water molecule have been investigated for molecular adsorption on MgO(100).[38−40] Our calculated binding energies are slightly higher than the values reported for molecular water adsorption on MgO(100).[38−41] Previous theoretical[39−41] studies of water adsorption on MgO(100) have also shown that dissociative adsorption of a single water molecule is an unfavorable process, and only the presence of three or four water molecules leads to dissociative adsorption stabilized by hydrogen-bonding due to lateral interaction from neighboring water molecules.

4. Discussion

4.1. Interpretation and Comparison to Previous Studies. Density functional theory calculations of the interaction of NO, NO_2, and CO_2 with BaO surfaces were previously published by several authors using either periodical-slab (Broqvist et al., $(\sqrt{2} \times \sqrt{2})$,[19] Broqvist et al. (3×3),[21] Schneider $(\sqrt{8} \times \sqrt{8})$,[20] or cluster (Broqvist et al.,[22] Karlsen et al.,[23] Branda et al.[24]) methods. There is quite some variation in these data. NO adsorption energies vary from -0.8[24] to -1.5 eV,[20] adsorption energies for NO_2 over an O_{surf} site vary from -0.8[22] to -1.5 eV,[20] and CO_2 adsorption energies vary from -1.7[23] to -2.3 eV.[20] In the case of NO_2, this discrepancy was pointed out by Broqvist et al.[21] and ascribed to be probably due to differences in allowed surface relaxation. Our studies on surface relaxation (Section 2) indicate that surface relaxation indeed plays a role, but its influence is too small ($\sim$0.25 eV difference in NO_2 adsorption energy between a nonrelaxed and a fully relaxed slab) to be at the origin of the variation observed in the literature. Instead, in the light of the results presented in Section 3, we believe that these variations can be explained to a large extent by the strong coverage-dependence of the adsorption energy. This is true for NO, NO_2, and CO_2, as discussed in the following.

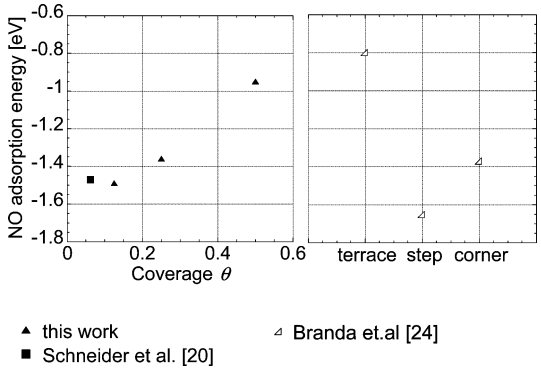

Figure 12. NO adsorption energy obtained from various studies. The left panel represents DFT periodical-slab calculations, the right panel DFT cluster calculations.

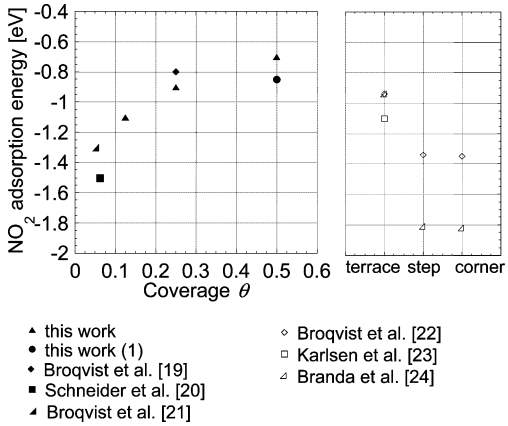

Figure 13. Adsorption energy of NO_2 over an O_{surf} site obtained from various studies. The left panel represent DFT periodical-slab calculations, the right panel DFT cluster calculations. (1) Adsorption energy after complete relaxation of the first slab layer.

A comparison of our calculated NO adsorption energy with previous studies is shown in Figure 12. While the geometrical parameters are similar in all studies (bond angle ~110°, short distances above the surface of ~150 pm, d(O−N) ~128 pm), the adsorption energies are quite different. For the periodic-slab calculations, the almost linear increase of adsorption energy with increasing surface coverage is obvious. Figure 13 shows calculated adsorption energies for NO_2 over an O_{surf} site versus coverage for various studies (see below for a discussion on other adsorption geometries). Again, the results of the various periodic-slab calculations fall together with the coverage dependent calculations performed in this study. A summary of data for CO_2 adsorption over an O_{surf} site is shown in Figure 14. All studies show the formation of the stable carbonate-type species. This is also indicated by the calculated OCO bond angles (Karlsen et al.: 130°; Schneider: 126°; this work: 125.8°; ideal carbonate: 120°). Again, the difference in adsorption energies can be explained from the influence of surface coverage.

Combining the results of all authors, Figures 12−14 clearly show the almost linear dependence of adsorption energy on surface coverage for all three species. The scatter in the data can be interpreted as an additional, smaller effect of surface relaxation: in our study, the two upper layers of a four-layer slab were relaxed and frozen; Schneider[20] uses a fully relaxed three-layer slab; Broqvist et al. use a nonrelaxed surface where only the adsorbent oxygen atom is geometry-optimized,[19] respectively, a fully relaxed first slab layer.[21] Figures 12−14 further illustrate the problem of comparing the results from cluster calculations. Here, a direct relation to a particular

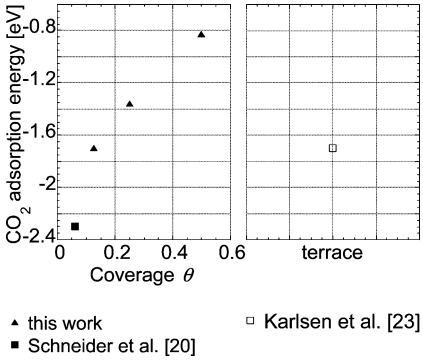

Figure 14. Adsorption energy of CO_2 over an O_{surf} site obtained from various studies. The left panel represents DFT periodical-slab calculations, the right panel represents DFT cluster calculations.

coverage of flat surfaces is not possible. The adsorption energy of a cluster terrace site seems to correspond rather accidentally to coverages of 0.5 in the case of NO, and to coverages of 0.125 in the case of NO_2 and CO_2.

The strong influence of coverage on adsorption energy is likely to be ascribed to adsorbate−adsorbate interactions. They can principally consist of through-space and through-surface interactions. As the adsorbate stability keeps increasing even for coverages <0.25, through-space interactions seem rather unlikely. Instead, surface-mediated effects from electron withdrawal by the adsorbates is probably the origin of this observation. Similar effects were observed by Broqvist et al. for NO_2 adsorption on $BaCO_3$,[16] and by Inderwildi et al. for rhodium surfaces.[33,43] This interpretation is supported also by the Mulliken charge analyses that were performed for our structures (Figures 3, 6, and 9): for each species, there is an almost linear relationship between adsorption energy and the charge exchanged between surface and adsorbate. This is indicative of the adsorbates' competition for slab electrons.

Different authors also studied various NO_2 adsorption geometries. Apart from the "N-down" geometry investigated here, Schneider and Broqvist et al. have additionally identified a nitrate-type species with short N−O_{surf} bonds and a bridged Ba_{surf}−ONO−Ba_{surf} species. All three geometries have different electronic structure,[21] but only a small difference in adsorption energy, ≤0.1 eV.[20,21] Both Broqvist et al. and Schneider also observed that pair formation of two NO_2 adsorbates leads to an additional stabilization on the order of 0.2−0.3 eV per molecule through electronic effects.[19,20] Evidently, there is a large variety of possible adsorption geometries for NO_2 on a BaO surface. However, the combined results from the various studies show that the difference in adsorption energy for various adsorption configurations is considerable smaller than that for various surface coverages.

4.2. Quantification of Surface Coverages. The calculations presented in the previous sections show that NO, NO_2, CO_2, and H_2O all have negative adsorption energies, i.e., they form stable adsorbates on a BaO(100) surface. The adsorption energies are, however, very different, and they furthermore strongly depend on surface coverage. These findings make it likely that carbon dioxide and water, both present as majority species in engine exhaust gases, adsorb on BaO in competition to the minority species NO and NO_2. They may thus play an important role in the NO_x storage mechanism, if not as chemically active species, then at least by blocking available surface sites.

To study the effects of the competitive adsorption of the four gas-phase species in a more quantitative way, we perform in

the following a computational analysis of the surface concentrations for a realistic exhaust gas composition. The model system consists of a total of 10 species: NO (gas), NO_2 (gas), CO_2 (gas), H_2O (gas), NO (ads, O-site), NO_2 (ads, O-site), NO_2 (ads, Ba-site), CO_2 (ads, carbonate-type), H_2O (ads), and free BaO surface sites that can undergo a total of five adsorption/desorption reactions. The adsorption/desorption equilibrium for each single surface species is given by

$$K = \theta_{\text{adsorbate}}/(p_{\text{gas-phase}}/p^0\,\theta_{\text{BaO}}) = \exp(-\Delta G_R(\theta_{\text{adsorbate}})/RT) \quad (2)$$

where K is the equilibrium constant, T is the temperature, $p_{\text{gas-phase}}$ is the gas-phase partial pressure, $p^0 = 101325$ Pa, θ_{BaO} is the fraction of free barium oxide surface sites, ΔG_R is the free enthalpy of the reaction, and R is the universal gas constant. Each of the five investigated adsorption/desorption reactions is described by one equation of type 2. The surface coverages are calculated by solving these equations under the boundary condition that the total surface coverage must not exceed unity.

To use the DFT results for evaluating eq 2, we make the following assumptions: (1) No surface species can exceed a coverage of unity. Here, the free (Ba_{surf} + O_{surf}) adsorption site pairs are respectively treated as one single species. This is a reasonable assumption, as the investigated molecules are considerably bigger than a single surface site (cf. Figures 1, 4, 7, and 10). Thus, each of the surface species in fact occupies a total of two surface sites (one Ba_{surf} and one O_{surf} site). The boundary condition for the total coverage is then

$$\theta_{\text{NO-O(surf)}} + \theta_{\text{NO}_2\text{-O(surf)}} + \theta_{\text{NO}_2\text{-Ba(surf)}} + \theta_{\text{CO}_2\text{-ads}} + \theta_{\text{H}_2\text{O-ads}} + \theta_{\text{BaO}} = 0.5 \quad (3)$$

(2) The free enthalpy ΔG_R can be obtained from the reaction enthalpy ΔH_R and the reaction entropy ΔS_R according to $\Delta G_R(T) = \Delta H_R(T) - T\Delta S_R(T)$. It is strongly temperature dependent. The DFT results presented in the previous section, however, correspond to $\Delta H_R(T = 0\ \text{K})$ only. To obtain the free enthalpy at realistic temperatures, a correction for the entropies are necessary (cf. refs 21, 44). This property is not known for the surface species in this study. Still, a simple approach based on kinetic theory allows estimation of the entropy of an adsorption/desorption reaction, when reasonable assumptions of the sticking coefficient and the desorption attempt frequency are made (see Appendix). For the following calculations, we therefore assume

$$\Delta G_R(T) = F\,E_{\text{ads,DFT}} - T\,\Delta_R S^{\text{estimated}}(T) \quad (4)$$

where F is Faraday's constant needed for the unit conversion of eV to J/mol. The calculation of $\Delta_R S^{\text{estimated}}(T)$ is given in the Appendix; it is negative by around 80−100 J/Kmol.

(3) The adsorption energies are assumed to depend on the coverage of the respective adsorbate only. Coadsorption effects such as energy gain through pair formation (cf. Section 4.1) are neglected. The coverage dependence is described using a simple linear relationship,

$$E_{\text{ads,DFT}} = E_{\text{ads}}{}^0 + \epsilon^*\,\theta \quad (5)$$

where the parameters $E_{\text{ads}}{}^0 = E_{\text{ads}}(\theta = 0)$ and ϵ are obtained by linear regression of the data shown in Figures 2, 5, 8, and 11. Their values are given in Table 5.

These assumptions represent considerable simplifications. They nevertheless allow calculation of the thermodynamic surface state versus temperature based on the results obtained from the DFT calculations. They thus enable a qualitative discussion of the species' competitive adsorption based on first principles. The complete mathematical description consists of a set of six coupled equations (five equations of type 1 and eq 2). They are solved numerically for a range of temperatures using a Newton algorithm.

TABLE 5: Linear Fit Parameters of the Coverage Dependence of NO, NO_2, CO_2, and H_2O (cf. eq 5)

	$E_{\text{ads}}{}^0$ (eV)	ϵ (eV)
NO (ads)	−1.69	1.46
NO_2−O_{surf} (ads)	−1.23	1.09
NO_2−Ba_{surf} (ads)	−1.43	1.72
CO_2 (ads)	−1.96	2.29
H_2O (ads)	−1.54	1.27

Calculation results are shown in Figure 15 for assumed gas-phase concentrations corresponding to typical lean engine operating conditions (250 ppm NO, 250 ppm NO_2, 7% CO_2, 10% H_2O). Over a large temperature range relevant for exhaust gas catalysis, the BaO surface is almost completely covered (total surface coverage ≥99% for temperatures ≤900 K). The main surface species are the carbonate-type CO_2 and H_2O, while the NO_x species have considerably lower coverages, in particular at elevated temperatures. With increasing temperature, the fraction of free BaO sites keeps increasing due to the increasing importance of the negative adsorption entropies.

Figure 16 shows similar calculations where CO_2 and H_2O are assumed to be absent. This corresponds to conditions studied before experimentally.[9-12] Over a wide range of temperatures, the surface is now completely covered with nitrogen oxide species (total surface coverage ≥90% for temperatures ≤700 K).

An important conclusion from these calculations is that the relatively large stability of involved species (CO_2, H_2O, NO, NO_2: E_{ads} < −0.7 eV) causes an almost complete (>99%)

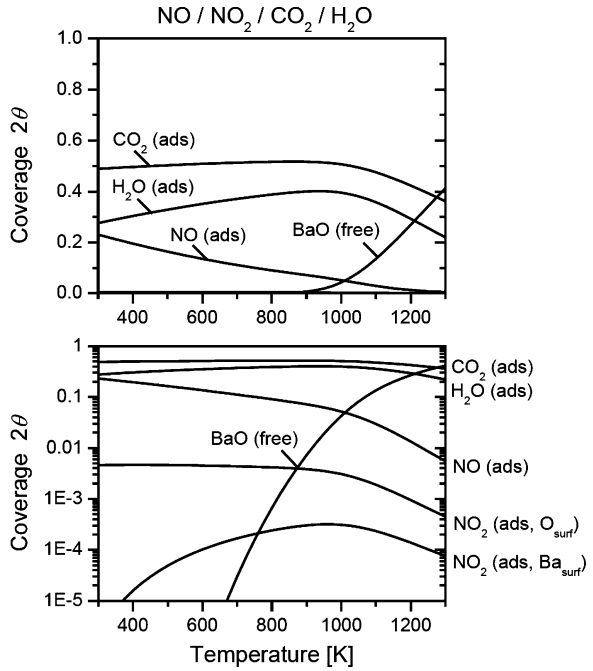

Figure 15. Equilibrium surface coverage for the ten-species system (four gas-phase species NO, NO_2, CO_2, and H_2O, five adsorbate species as given in Table 5 plus free BaO surface sites) simulated for a typical lean engine exhaust gas (250 ppm NO, 250 ppm NO_2, 7% CO_2, 10% H_2O) vs temperature. Both panels show the same data on different scales. The coverage is given in units of 2θ because each species is assumed to occupy one (BaO) surface pair.

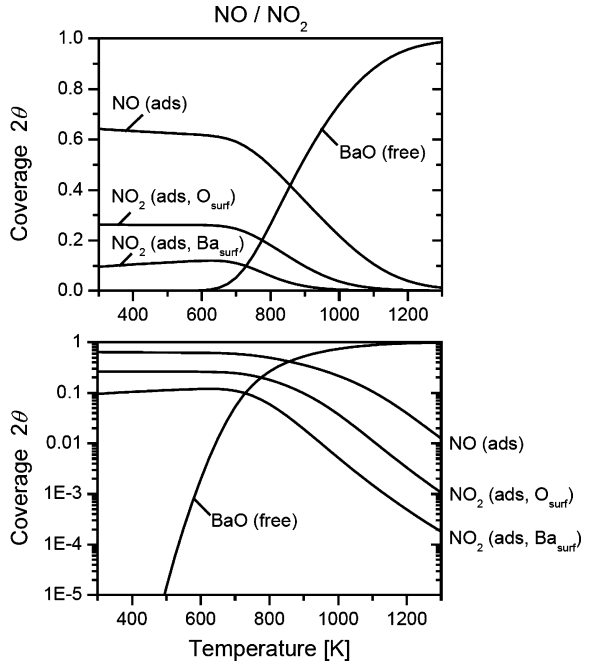

Figure 16. Equilibrium surface coverage for the ten-species system for a gas atmosphere without carbon dioxide and water (250 ppm NO, 250 ppm NO_2) vs temperature. Both panels show the same data on different scales. The coverage is given in units of 2θ because each species is assumed to occupy one (BaO) surface pair.

coverage of the surface at temperatures relevant for exhaust gas catalysis. As the thermodynamic surface state is the setting under which storage kinetics must take place, this needs to be taken into account when considering mechanistic aspects of NO_x storage: (1) Reactions between two surface-attached species (e.g., the disproportionation reaction $2NO_2$ (ads) $\rightarrow$ NO (ads) + NO_3 (ads) as proposed by Broqvist et al. [19]) are more likely than simple surface dissociation reactions that require the presence of free surface sites (e.g., NO_2 (ads) + free site $\rightarrow$ NO (ads) + O (ads)). Pair formation effects, as for example, studied by Schneider and Broqvist et al.,[19,20] are likely to play an important role. (2) NO_x storage may be kinetically controlled through the availability of free surface sites for adsorption of reactants. (3) For further mechanistic studies, quantum chemical calculations should be performed in the limit of highly covered surfaces. Periodic-slab calculations using isolated molecules on large supercells (e.g., the large supercells of Schneider[20] and Broqvist[21]) or cluster calculations do not seem to represent realistic conditions. (4) The observation of high coverages of carbonate-type adsorbates supports the possibility of barium carbonate (instead of barium oxide) being the active storage species under realistic gas-phase compositions.

5. Summary

The adsorption of four gas-phase species important in automotive exhaust gas catalysis (NO, NO_2, CO_2, and H_2O) on a BaO storage catalyst surface were investigated with quantum chemical calculations based on density functional theory. Adsorption geometries and energies were calculated in dependence of surface coverage. All species form stable adsorbates on the BaO(100) surface. The adsorption energies strongly depend on surface coverage through electronic effects. The most important observations are summarized as follows. (1) NO adsorbs as stable nitrite-like species. (2) NO_2 may adsorb in various geometries on both, barium and oxygen surface sites. Variation in adsorption energy for different geometries at constant coverage is considerably smaller (~25%) than for varying surface coverage (~100% increase between coverages of 0.5 and 0.125). This observation allows explanation of the disagreement of calculated adsorption energies in the existing literature. (3) Upon interaction of CO_2 with a BaO surface, a very stable ($E_{ads}(\theta = 0.125) = -1.7$ eV) chemisorbed state of CO_2 was identified where the adsorbate together with one surface oxygen atom forms a carbonate-type structure. The adsorption of this species from the gas-phase is nonactivated. (4) H_2O adsorbs strongly on BaO surface, with adsorption energies in the same range as NO, NO_2, and CO_2.

Numerical thermodynamic calculations of the competitive adsorption/desorption equilibria of the four gas-phase species under realistic engine exhaust gas conditions show that the surface is almost completely covered with carbon dioxide and water over a wide range of temperatures. The results indicate that these species play an essential role in the surface processes during NO_x storage on BaO, where they can block a large part of available surface sites. This finding also supports the possibility of barium carbonate being the active storage species under realistic gas-phase compositions.

Acknowledgment. We thank Dirk Lebiedz (Heidelberg University), Olaf Deutschmann (Karlsruhe University), Wojciech Grochala (ICM, Warsaw University), and Jerzy Gorecki (ICM, Warsaw University) for helpful discussions and support of this work. M.T. acknowledges funding by the Deutsche Forschungsgemeinschaft through the International Graduate College 710.

Appendix: Estimation of Adsorption Entropy

To calculate free adsorption energy ΔG_R using the results of the DFT calculations, values for the adsorption entropy ΔS_R are needed. We estimate these values based on kinetic theory using certain reasonable assumptions, as given in the following. This approach is similar to what was used by Broqvist et al.[21] for calculation of temperature-dependent coverages.

Following from transition state theory, the forward and reverse rates k_f and k_r (1/s) for a chemical reaction (here: adsorption/desorption reaction) are given by

$$k_f = k_f^0 \exp\left(-\frac{E_f^{act}}{RT}\right) \quad (6)$$

$$k_r = k_r^0 \exp\left(-\frac{E_r^{act}}{RT}\right) \quad (7)$$

where k_f^0 and k_r^0 (1/s) are the preexponential factors and E_f^{act} and E_r^{act} (J/mol) are the thermal activation energies of forward and reverse reactions, respectively. The relationship between these kinetic data and the thermodynamical reaction parameters are given by

$$k_f^0/k_r^0 = \exp(\Delta S_R/R) \quad (8)$$

$$E_f^{act} - E_r^{act} = \Delta H_R \quad (9)$$

i.e., the reaction entropy is related to the preexponential factors, and the reaction enthalpy (which is available from DFT calculations) is related to the activation energies.

For a surface adsorption reaction, k_f^0 can be calculated based on kinetic gas theory from the number of gas-phase molecule/surface collisions, weighed with the dimensionless sticking

coefficient S, which is the probability that a collision leads to an adsorption. This results in[45,46]

$$k_f^0 = S\frac{p^0}{\Gamma}(2\pi MRT)^{-1/2} \quad (10)$$

where $p^0 = 101\,325$ Pa, Γ is the surface density of adsorption sites (here we use a value of 5.37×10^{-6} mol/m^2, following from the lattice constant of the Ba(100) surface), M (kg/mol) is the molar mass of the adsorbing molecule, R is the universal gas constant, and T (K) is the temperature.

For a surface desorption reaction, it can be assumed that k_r^0 represents the so-called attempt frequency, i.e., the vibrational frequency of the adsorbed species in the direction perpendicular to the surface. Under the assumption that the adsorbed species and the transition state of the desorption reaction have the same partition function, i.e., the same degrees of freedom[47] (which is a reasonable assumptions for a strongly adsorbed species), it can be estimated that[47]

$$k_r^0 = \frac{kT}{h} \quad (11)$$

where k is the Boltzmann constant and h is Planck's constant.

Equations 8, 10, and 11 allow calculation of the temperature-dependent entropy of the adsorption/desorption reaction when the sticking coefficient S is known. We assume in our calculations constant sticking coefficients of unity for all species, which is a common assumption for chemisorbed species.

Using this approach, calculated reaction entropies for NO_2 adsorption/desorption, for example, vary between -76 J/Kmol at 300 K and -94 J/Kmol at 1300 K. The entropies are quite negative, which is typical for an adsorption reaction:[45] the largest part of the gas-phase molecule's entropy comes from translational motion, which is lost upon chemisorption.

References and Notes

(1) Heck, R. M.; Farrauto, R. J. *Appl. Catal., A* **2001**, *221*, 443.
(2) Shelef, M. *Chem. Rev.* **1995**, *95*, 209.
(3) Sedlmair, C.; Seshan, K.; Jentys, A.; Lercher, J. A. *J. Catal.* **2003**, *214*, 308.
(4) Schmitz, P. H.; Baird, R. J. *J. Phys. Chem. B* **2002**, *106*, 4172.
(5) Fridell, E.; Persson, H.; Westerberg, B.; Olsson, L.; Skoglundh, M. *Catal. Lett.* **2000**, *66*, 71.
(6) Olsson, L.; Persson, H.; Fridell, E.; Skoglundh, M.; Andersson, B. *J. Phys. Chem. B* **2001**, *105*, 6895.
(7) Tuttlies, U.; Schmeisser, V.; Eigenberger, G. *Top. Catal.* **2004**, *30/31*, 187.
(8) Rodriguez, F.; Juste, L.; Potvin, C.; Tempère, J. F.; Blanchard, G.; Djéga-Mariadassou, G. *Catal. Lett.* **2001**, *72*, 59.
(9) Prinetto, F.; Ghiotti, G.; Nova, I.; Lietti, L.; Tronconi, E.; Forzatti, P. *J. Phys. Chem. B* **2001**, *105*, 12732.
(10) Kabin, K. S.; Muncrief, R. L.; Harold, M. P. *Catal.s Today* **2004**, *96*, 79.
(11) Su, Y.; Amiridis, M. D. *Catal. Today* **2004**, *96*, 31.
(12) Broqvist, P.; Grönbeck, H.; Fridell, E.; Panas, I. *Catal. Today* **2004**, *96*, 71.
(13) Nova, I.; Castoldi, L.; Lietti, L.; Tronconi, E.; Forzatti, P. *Catal. Today* **2002**, *75*, 431.
(14) Huang, H. Y.; Long, R. Q.; Yang, R. T. *Energy Fuels* **2001**, *15*, 205.
(15) Hilgendorff, M. *Top. Catal.* **2004**, *30/31*, 155.
(16) Broqvist, P.; Panas, I.; Grönbeck, H. *J. Phys. Chem. B* **2005**, *109*, 9613.
(17) Grönbeck, H. *Top. Catal.* **2004**, *28*, 59.
(18) Ge, Q.; Kose, R.; King, D. A. *Adv. Catal.* **2000**, *45*, 207.
(19) Broqvist, P.; Panas, I.; Fridell, E.; Persson, H. *J. Phys. Chem. B* **2002**, *106*, 137.
(20) Schneider, W. F. *J. Phys. Chem. B* **2004**, *108*, 273.
(21) Broqvist, P.; Panas, I.; Grönbeck, H. *J. Phys. Chem. B* **2005**, *109*, 15410.
(22) Broqvist, P.; Grönbeck, H.; Fridell, E.; Panas, I. *J. Phys. Chem. B* **2004**, *108*, 3523.
(23) Karlsen, E. J.; Nygren, M. A.; Pettersson, L. G. M. *J. Phys. Chem. B* **2003**, *107*, 7795.
(24) Branda, M. M.; Di Valentin, C.; Pacchioni, G. *J. Phys. Chem. B* **2004**, *108*, 4752.
(25) Perdew, J. P.; Burke, K.; Ernzerhof, M. *Phys. Rev. Lett.* **1996**, *77*, 3865.
(26) Inderwildi, O. R.; Lebiedz, D.; Deutschmann, O.; Warnatz, J. *J. Chem. Phys.* **2005**, *122*, 034710.
(27) Segall, M. D.; Lindan, P. J. D.; Probert, M. J.; Pickard, C. J.; Hasnip, P. J.; Clark, S. J.; Payne, M. C. *J. Phys.: Condens. Matter* **2002**, *14*, 2717.
(28) Perdew, J. P.; Chevary, J. A.; Vosko, S. H.; Jackson, K. A.; Pederson, M. R.; Fiolhais, C. *Phys. Rev. B* **1992**, *46*, 6671.
(29) Vanderbilt, D. *Phys. Rev. B* **1990**, *41*, 7892.
(30) Monkhorst, H. J.; Pack, J. D. *Phys. Rev. B* **1976**, *13*, 5188.
(31) Segall, M. D.; Shah, R.; Pickard, C. J.; Payne, M. C. *Phys. Rev. B* **1996**, *54*, 16317.
(32) Govind, N.; Petersen, M.; Fitzgerald, G.; King-Smith, D.; Andzelm, J. *Comput. Mater. Sci.* **2003**, *28*, 250.
(33) Inderwildi, O. R.; Lebiedz, D.; Deutschmann, O.; Warnatz, J. *J. Chem. Phys.* **2005**, *122*, 154702.
(34) Prinetto, F.; Ghiotti, G.; Nova, I.; Castodli, L.; Lietti, L.; Tronconi, E.; Forzatti, P. *Phys. Chem. Chem. Phys.* **2003**, *5*, 4428.
(35) Holleman, A. F.; Wiberg, E. *Lehrbuch der Anorganischen Chemie*; Walter de Gruyter: Berlin, New York, 1995; Vol. 101.
(36) *Surface and Near-Surface Chemistry of Oxide Materials*; Nowotny, J.,; Dufour, L., Eds.; Elsevier: New York, 1988.
(37) Yu, Y.; Guo, Q.; Liu, S.; Wang, E. *Phys. Rev. B* **2003**, *68*, 115414.
(38) Scamehorn, C. A.; Harrison, N. M.; McCarthy, M. I. *J. Chem. Phys.* **1994**, *101*, 1547.
(39) Odelius, M. *Phys. Rev. Lett.* **1999**, *82*, 3919.
(40) Tikhomirov, V. A.; Jug, K. *J. Phys. Chem. B* **2000**, *104*, 7619.
(41) Giordano, L.; Goniakowski, J.; Suzanne, J. *Phys. Rev. Lett.* **1998**, *81*, 1271.
(42) Cho, J.-H.; Park, J. M.; Kim, K. S. *Phys. Rev. B* **2000**, *62*, 9981.
(43) Inderwildi, O.; Lebiedz, D.; Warnatz, J. *Phys. Chem. Chem. Phys.* **2005**, *7*, 1.
(44) Nørskov, J. K.; Rosslmeisl, J.; Logadottir, A.; Lindqvist, L.; Kitchin, J. R.; Bligaard, T.; Jónsson, H. *J. Phys. Chem. B* **2004**, *108*, 17886.
(45) Kee, R. J.; Coltrin, M. E.; Glarborg, P. *Chemically Reacting Flow: Theory and Practice*; John Wiley & Sons: New York, 2003.
(46) Behrendt, F.; Deutschmann, O.; Ruf, B.; Schmidt, R.; Warnatz, J. Simulation of Heterogeneous Reaction Systems. In *Gas-Phase Chemical Reaction Systems: Experiment and Models, 100 Years after Max Bodenstein*; Wolfrum, J., Volpp, H.-R., Rannacher, R., Warnatz, J., Eds.; Springer: New York, 1996; p 265.
(47) Christmann, K. *Surface Physical Chemistry*; Steinkopff: Darmstadt, Germany, 1991.
(48) Galasso, F. S. *Structure and Properties of Inorganic Solids*; Pergamon Press: Oxford, 1970.